

# The Diurnal Cycle of Convection and Atmospheric Tides in an Aquaplanet GCM

S. J. WOOLNOUGH AND J. M. SLINGO

*Centre for Global Atmospheric Modelling, Department of Meteorology, University of Reading, Reading, United Kingdom*

B. J. HOSKINS

*Department of Meteorology, University of Reading, Reading, United Kingdom*

(Manuscript received 6 November 2003, in final form 18 March 2004)

## ABSTRACT

The diurnal cycle of tropical convection and its relationship to the atmospheric tides is investigated using an aquaplanet GCM.

The diurnal and semidiurnal harmonics of precipitation are both found to contribute significantly to the total diurnal variability of precipitation in the model, which is broadly consistent with observations of the diurnal cycle of convection over the open ocean. The semidiurnal tide is found to be the dominant forcing for the semidiurnal harmonic of precipitation. In contrast the diurnal tide plays only a small role in forcing the diurnal harmonic of precipitation, which is dominated by the variations in shortwave and longwave heating. In both the diurnal and semidiurnal harmonics, the feedback onto the convection by the humidity tendencies due to the convection is found to be important in determining the phase of the harmonics. Further experiments show that the diurnal cycle of precipitation is sensitive to the choice of closure in the convection scheme.

While the surface pressure signal of the simulated atmospheric tides in the model agree well with both theory and observations in their magnitude and phase, sensitivity experiments suggest that the role of the stratospheric ozone in forcing the semidiurnal tide is much reduced compared to theoretical predictions. Furthermore, the influence of the cloud radiative effects seems small. It is suggested that the radiative heating profile in the troposphere, associated primarily with the water vapor distribution, is more important than previously thought for driving the semidiurnal tide. However, this result may be sensitive to the vertical resolution and extent of the model.

## 1. Introduction

The diurnal<sup>1</sup> cycle of solar insolation provides a strong forcing of variability on the climate system. The climate system responds to this forcing in a number of ways, including significant diurnal variations in tropical precipitation and surface pressure (a manifestation of the atmospheric tides). This paper explores the relationship between the diurnal cycle of precipitation and the atmospheric tides in the context of an idealized atmospheric model.

While there are a number of studies of the diurnal cycle of precipitation over land [see, e.g., Dai (2001)

for a summary], until recently, the scarcity of observational data over the oceans has meant that detailed studies of the oceanic diurnal cycle of convection have been difficult. Following the advent of satellite observations, a more global picture of the diurnal cycle of convection has developed (e.g., Janowiak et al. 1994; Yang and Slingo 2001). These studies have used satellite radiances to infer properties of the cloud field and then to relate these cloud fields to the precipitation. Direct comparisons between in situ observations and satellite observations over both ocean and land (e.g., McGarry and Reed 1978; Janowiak et al. 1994) and a recent modeling study by Slingo et al. (2004) suggest that precipitation peaks some 2–3 h before cold cloud maxima. Such an effect has implications for estimates of the phase of the diurnal cycle of precipitation made from satellite observations. More recently the use of spaceborne rain radar and passive microwave instruments as part of the Tropical Rainfall Measuring Mission (TRMM) has allowed an analysis of the diurnal cycle of a more directly measured precipitation dataset over the global Tropics (e.g., Nesbitt and Zipser 2003). However, because of the temporal resolution of the TRMM

---

<sup>1</sup> In this paper the word diurnal will be used to describe variations with periods of 24 h or less, *except* in the phrases “diurnal harmonic” and “diurnal tide” where it will refer to variations with a period of 24 h only.

---

*Corresponding author address:* Dr. S. J. Woolnough, Centre for Global Atmospheric Modelling, Department of Meteorology, University of Reading, P.O. Box 243, Earley Gate, Reading RG6 6BB, United Kingdom.  
E-mail: S.J.Woolnough@reading.ac.uk

dataset in the Tropics (approximately one observation at any point every two days) the diurnal cycle is subsampled and there is a risk of aliasing longer-time-scale variability onto the diurnal cycle.

Within the limits imposed by the observational and analysis techniques a relatively consistent picture of the diurnal variability of tropical precipitation has developed. Over the tropical landmasses convective precipitation is generally thought to peak in late afternoon and early evening, primarily driven by the daytime heating of the boundary layer. However, there are regional variations that suggest, for example, that orography and the presence of mesoscale convective systems may play a role in determining the timing of convection (e.g., Yang and Slingo 2001; Nesbitt and Zipser 2003).

Over the oceans the diurnal cycle of precipitation is much smaller in magnitude with an amplitude corresponding to about 15% of the daily mean rate (e.g., Nesbitt and Zipser 2003). Over the open ocean away from the influence of land the precipitation typically peaks in the early hours of the morning (e.g., Gray and Jacobson 1977; Yang and Slingo 2001; Nesbitt and Zipser 2003). Nesbitt and Zipser (2003) found a late afternoon minimum in oceanic precipitation, suggesting that the diurnal cycle in precipitation has significant contributions from higher harmonics than the diurnal harmonic. Yang and Slingo (2001) found that around the coastal areas there are interesting signals of propagation of the phase of the diurnal cycle of convection, probably associated with the land–sea breeze circulations. The influence of these may spread for hundreds of kilometers. In some warmer ocean areas the observations suggest that at least at times, particularly in undisturbed conditions, the diurnal cycle of convection may be more characteristic of the land diurnal cycle with convective maxima in late afternoon and early evening (Sui et al. 1997; Yang and Slingo 2001), possibly indicating a role for the underlying ocean surface in driving the diurnal variations in these regions.

The relatively poor observational data of the diurnal cycle of convection and, in particular, the fields potentially related to its cause over the ocean has made determining the mechanisms of the oceanic diurnal cycle difficult. A number of hypotheses for the later peak in convection over the ocean have been proposed including nighttime destabilization of the profile by infrared cooling of the clouds as opposed to daytime stabilization of the profile by shortwave absorption (Randall et al. 1991), vertical circulations induced by differences in cloudy and cloud-free heating rates (Gray and Jacobson 1977), and the lifetime associated with convective systems triggered in the afternoon by near-surface heating (Chen and Houze 1997).

Many of the possible mechanisms for producing a diurnal cycle in convection may be poorly represented or absent in GCMs; however, there are limited studies of the modeled diurnal cycle of precipitation. Yang and Slingo (2001) and Slingo et al. (2004) have made com-

parisons of the Met Office Unified Model diurnal cycle of convection with satellite observations. They found that over land convective precipitation in GCMs typically peaks too early in the day, often before noon. Over the ocean the model was able to reproduce at least the gross features of the diurnal cycle of convection with a maximum in the early hours of the morning. However, it was generally unable to capture the regional variations associated with land–sea breezes and surface-forced diurnal cycles as these processes are not represented in the model. Dai and Trenberth (2004) found broadly similar behavior of the diurnal cycle of convection in a study of the Community Climate System Model.

In contrast to the diurnal cycle of precipitation, the diurnal variations of surface pressure or “atmospheric tides” and the processes that drive the atmospheric tides are generally considered to be well understood. Chapman and Lindzen (1970) reported early observations of the atmospheric tides (e.g., Haurwitz 1956, 1965) and largely accounted for their amplitude and phase by considering the dynamical response (through the generation and propagation of internal gravity waves) to the diurnal and semidiurnal harmonics of solar heating.

The semidiurnal tide has a surface pressure signal peaking at the equator, decaying with latitude as approximately  $\cos^3\phi$ . It is a westward propagating zonal wavenumber-2 signal with some longitudinal variations in amplitude and phase within the Tropics. Haurwitz (1956) found that an equatorial amplitude of 1.16 mb best described his data, with maxima at around 0945 and 2145 LT. A more recent study by Dai and Wang (1999) found spatial variations of the order of 20% in the amplitude of the semidiurnal tide but was generally in agreement with earlier observations.

The surface pressure signal of the diurnal tide has a smaller amplitude: Haurwitz (1965) found an amplitude of 0.593 mb with a maximum around 0500 LT for the zonal wave-1 traveling wave. However, the amplitude and phase of the surface pressure signal of the diurnal tide shows much larger longitudinal and temporal variations. For example, Dai and Wang (1999) found amplitudes in excess of 1 mb for the diurnal harmonic of surface pressure over the tropical continents and North America.

The generally large amplitude of the semidiurnal harmonic of surface pressure compared to the diurnal harmonic (despite the larger diurnal harmonic of the solar forcing) have been explained by consideration of the propagation characteristics of the wave modes responsible for the tides. Most of the forcing of the diurnal harmonic projects onto wave modes that are vertically trapped. As a result the surface pressure signal is mainly a response to tropospheric heating. The theoretical calculations discussed in the review of Chapman and Lindzen (1970) underpredict the amplitude of the surface pressure signal of the diurnal tide by about 30%. However, Braswell and Lindzen (1998) reported that possible discrepancies between radiative models and observa-

tions might largely account for the differences between the predicted and observed magnitude of the diurnal tide. Because the diurnal harmonic of surface pressure is largely driven by tropospheric heating, there can be large spatial variations in the forcing, associated with variations in the absorption of the shortwave radiation by clouds and water vapor. Other sources of heating with large spatial inhomogeneities in their diurnal harmonics (e.g., sensible heat transfer from the surface or latent heating) may contribute to the forcing of the diurnal tide.

In contrast the wave modes responsible for the semi-diurnal tide have a large vertical wavelength and as such interfere constructively, leading to a large signal at the surface. According to the theory discussed in Chapman and Lindzen (1970), the deep heating that forces these waves is dominated by the ozone heating in the stratosphere: they predict that about 70% of the semidiurnal surface pressure signal is forced by this ozone heating. There are some small discrepancies between the predicted semidiurnal tide and that observed, including a phase error of about 45 min. Lindzen (1978) and Hamilton (1981) have suggested that these discrepancies can be accounted for if, in addition, there is a semidiurnal harmonic of latent heating corresponding to a semidiurnal harmonic of precipitation of about 1.2 mm day<sup>-1</sup> with a maximum about 0330 LT. Limited observations available at the time of their studies showed evidence of a semidiurnal harmonic of precipitation with approximately the correct phase and amplitude to account for the phase error and some other discrepancies in the earlier predictions. A more recent study by Dai (2001) with a much larger dataset of weather reports confirmed the existence of a semidiurnal harmonic in the frequency of showery precipitation with the required phase, but was not able to comment on the magnitude of any precipitation anomaly associated with this mode. Lindzen (1978) argued that the convergence associated with the semidiurnal tide was too small and of the wrong phase to drive the the semidiurnal harmonic of precipitation required from his calculations. However, he did not rule out the possible role of the semidiurnal tide in providing a trigger for the semidiurnal harmonic of precipitation.

In this paper the diurnal cycle of convection and the atmospheric tides are investigated using an aquaplanet version of the Met Office Unified Model. With prescribed zonally uniform sea surface temperatures this provides a relatively simple method to explore the basic diurnal response of the model over tropical oceans. The relative importance of different aspects of the explicit and parameterized physics, including the role of the atmospheric tides in the diurnal cycle of precipitation, can be assessed and the sensitivity to the parameterization techniques can be explored. These experiments are the first step in understanding the diurnal cycle of convection over the oceans in the full model. In particular they provide an understanding of the basic response of the model to the diurnal forcing against which the

role of variations in the forcing (e.g., the proximity to land masses or the effect of a diurnal cycle in SST) in determining the diurnal cycle of convection in the full model can be addressed. As more confidence is gained in the observations of the diurnal cycle of precipitation, the understanding obtained in studies such as that described here should enable changes to the parameterization in full GCMs leading to improved performance.

The model and some aspects of its climatology are described in section 2 along with a description of the technique for isolating the diurnal cycle. The diurnal cycle of convection and the surface pressure signal of the atmospheric tides<sup>2</sup> in the model are described in section 3 and the relationship between them discussed. A more detailed analysis of the behavior of the convection scheme and its response to the diurnal forcing is presented in section 4. The implications of the results are discussed in section 5.

## 2. Model description

The numerical model used in this study is an aquaplanet version of the Met Office Unified Model version HadAM3 (Hadley Centre Atmospheric Model). A detailed description of the components of the model can be found in Pope et al. (2000) and references therein. The model is run with a horizontal resolution of 2.5° latitude and 3.75° longitude with 30 levels in the vertical, corresponding to a layer thickness of about 50 hPa in the midtroposphere, with higher resolution in the boundary layer and around the tropopause. There are five model levels above 100 hPa at approximately 77, 52, 30, 15, and 4.5 hPa. A  $\nabla^6$  horizontal damping with a time scale equivalent to 12 h on the shortest resolved wavelength is applied at all the levels except the top level where it is replaced by a  $\nabla^2$  damping with a time scale of 1 h on the shortest resolved wavelength. For wavelengths that dominate the tidal forcing ( $\sim 4000$  km or greater) the damping time scale is in excess of 1 day in the top level. The upper boundary condition ( $Dp/Dt = 0$ ) is applied at  $p = 0.5$  hPa.

Because of the nature of the present study it is worth summarizing the convection scheme here. It is the mass-flux scheme of Gregory and Rowntree (1990) including a representation of convective downdrafts (Gregory and Allen 1991) and the vertical transport of momentum by convection (Gregory et al. 1997). The scheme uses a bulk cloud model, based on parcel theory and taking into account the effects of mixing entrainment and detrainment between the cloud parcel and the environment, to represent an ensemble of convecting plumes within the grid box.

Convection is initiated if a parcel with a prescribed small buoyancy excess (equivalent to 0.2 K) in one layer

<sup>2</sup> In the following sections references to the amplitude and phase of the tides will refer to the surface pressure signal associated with the tide.

retains its buoyancy excess after lifting to the next layer, taking account of latent heat release and entrainment of environmental air. Once convection is initiated the parcel continues to ascend, mixing by entrainment and detrainment with the environmental air. If the parcels buoyancy excess falls below the critical value on lifting from level  $k$  to  $k + 1$ , then a proportion of the cloud parcel is detrained into level  $k$ , such that the parcel's buoyancy excess in level  $k + 1$  is greater than the critical value. This forced detrainment represents the termination of less buoyant plumes within the ensemble. The convection is terminated at the zero buoyancy level of an undiluted parcel lifted from the initial convective starting level, or if the mass flux falls below a prescribed minimum level. On termination of the convection, the convecting plume is detrained into the termination level and the level above. The initial mass flux is determined from the buoyancy excess of the parcel after lifting from the initiation level to the next level. The environmental profiles of moisture, temperature, and momentum are modified by the effects of the detrainment and the compensating subsidence within the cloud-free area. The downdraft scheme works in the same way, but for an inverted plume. The negative buoyancy of the downdraft is maintained by evaporation of falling precipitation.

As well as the standard buoyancy closed version of the scheme, an alternative closure is available, based on requiring the convection to remove convective available potential energy (CAPE) from the profile on a prescribed time scale with the mass flux being scaled to achieve this rate of change of CAPE.

The aquaplanet model has been successfully used to investigate aspects of tropical intraseasonal variability of convection associated with the Madden-Julian oscillation (e.g., Woolnough et al. 2001; Inness et al. 2001).

#### Experimental technique

The control integration of the model is a 90-day integration with the buoyancy-based closure for the convection scheme, forced by a zonal mean SST given by

$$\text{SST} = 29^{\circ}\text{C} - 29^{\circ}\text{C} \left[ \frac{\sin^2(\phi/60^{\circ}) + \sin^4(\phi/60^{\circ})}{2} \right]$$

between  $\pm 60^{\circ}$  of latitude and  $0^{\circ}\text{C}$  poleward of this. This profile is used by Woolnough et al. (2001) and Inness et al. (2001) as representative of the SST profile in the Indo-Pacific warm pool region. The solar forcing is fixed to the March equinox conditions and the ozone climatology is a zonally symmetric version of the climatology of Li and Shine (1995). The model's ozone profile is constructed from a mass-weighted integral of the ozone climatology within each model layer (rather than by interpolation) to conserve the total column ozone.

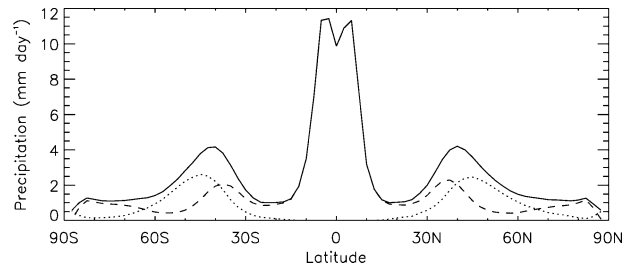


FIG. 1. Zonal mean precipitation climatology from 90 days of the control integration. The solid line shows the total precipitation, the dashed line shows the precipitation from the convection scheme, and the dotted line shows the precipitation from the large-scale cloud scheme.

In addition to the control integration a number of sensitivity experiments were performed with either alterations in the nature of the diurnal forcing or changes to the closure of the convection scheme.

Figure 1 shows the zonal mean precipitation climatology of the control integration of the model. The precipitation has a broad maximum  $10^{\circ}$  either side of the equator with a slight local minimum on the equator. The maximum zonal mean precipitation rates are around  $10\text{--}12\text{ mm day}^{-1}$ , which is comparable to the observed precipitation rates in the tropical western Pacific. The tropical precipitation is almost completely produced by the parameterized convection rather than the large-scale rain.

To efficiently isolate the diurnal cycle of a field, the diurnal and semidiurnal harmonics were calculated at each grid point from 3-hourly mean diagnostics, and composite harmonics produced by averaging these harmonics at each grid point accounting for the longitudinal variations in local time of day. The use of 3-hourly mean diagnostics can be shown to result in an amplitude loss of 2.5% and 10% for the diurnal and semidiurnal harmonics, respectively, compared to using instantaneous fields.

### 3. The diurnal cycle of surface pressure and precipitation

Figure 2 shows the composite diurnal and semidiurnal harmonics of surface pressure and precipitation for the control integration. Also shown is the sum of these two precipitation harmonics, which gives about 80% of the variability associated with the diurnal cycle of precipitation in this model. As indicated on the figure, these composites may be viewed in two ways, either as a horizontal plot of the 3-h mean anomalies associated with each harmonic for the period 2100–0000 UTC, or as a time–latitude plot at a particular longitude.

The magnitude and phase of the semidiurnal tide in this model is in good agreement with the observed semidiurnal tide, with an amplitude of 1.15 hPa and maxima at 0930 and 2130 local time (LT). The diurnal tide has an amplitude of about 0.38 hPa, which is less than ob-

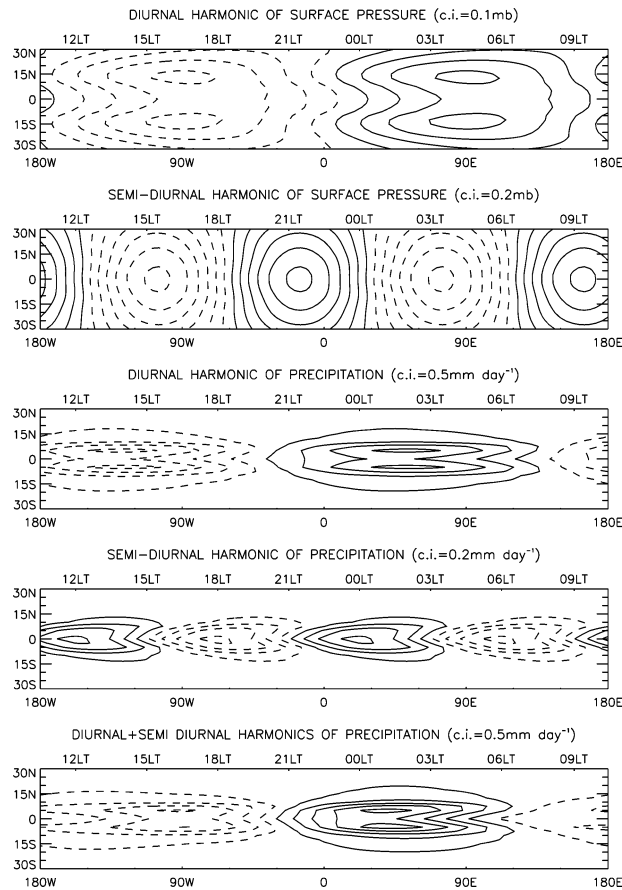


FIG. 2. Composite diurnal and semidiurnal harmonics of surface pressure and precipitation from the control integration. (bottom) The sum of the diurnal and semidiurnal harmonics of precipitation. The lower horizontal axis represents the longitude for the averaging period 2100–0000 UTC, and the upper axis represents local time for a particular longitude. The contour intervals are shown on the figure; for each plot the contours are offset from zero by half the contour interval, and negative contours are dashed.

served [and similar to the theory reported in Chapman and Lindzen (1970)] but its phase, with a maximum at around 0545 LT, is consistent with both observations and theory. The meridional structure of the diurnal tide, with off-equatorial peaks, is in contrast to both theory and observations, which suggest an equatorial maximum in the amplitude of the tide. However, a significant negative contribution from the propagating modes, which have a similar meridional structure to the latent heating (and associated cloud cover) in the Tropics, could modify the surface response in this way.

The diurnal cycle of precipitation, with a magnitude of about  $2 \text{ mm day}^{-1}$ , accounts for only 3%–4% of the total variance in this integration. These figures are small in comparison to the 15%–20% of the total variance in brightness temperature explained by intradiurnal time scales and an implied diurnal cycle of precipitation of between 3–6  $\text{mm day}^{-1}$  found by Yang and Slingo (2001), but the magnitude is comparable to that of the

diurnal cycle of precipitation over the oceanic regions in the full version of this model and in reasonable agreement with the 15% of the daily mean observed by Nesbitt and Zipser (2003) over oceanic regions based on TRMM data.

The diurnal harmonic of precipitation has its maximum amplitude off the equator, collocated with the maximum in the mean precipitation, with a magnitude of  $1.9 \text{ mm day}^{-1}$  corresponding to about 15% of the mean precipitation at this location, occurring at about 0130 LT. The magnitude of the diurnal harmonic shows larger latitudinal variations than the mean precipitation and the maximum on the equator is about  $1.3 \text{ mm day}^{-1}$ . The semidiurnal harmonic of precipitation has its largest signal on the equator with an amplitude of  $0.75 \text{ mm day}^{-1}$ , corresponding to about 7.5% of the mean daily precipitation, and with maxima at around noon and midnight. This combination gives a diurnal cycle that shows a strong peak in precipitation during the early hours of the morning (between 0000 and 0300 LT) and a broader, weaker minimum in precipitation in the late afternoon (between 1500 and 1800 LT).

The phase of the diurnal harmonic of precipitation is consistent with the limited observations over open ocean areas. The modeled semidiurnal harmonic of precipitation does not agree well with the phase of the few reported observations of the semidiurnal harmonic of precipitation, but these observations are based either on a limited number of stations or on precipitation frequency rather than amount. Hence, comparisons between the model and these observations may not be useful.

Understanding the diurnal cycle of precipitation in this model clearly requires an understanding of both semidiurnal and diurnal harmonics of precipitation. The phase relationships between the semidiurnal harmonics of precipitation and surface pressure are very different from those of the diurnal harmonics of these fields. The maximum of the diurnal harmonic of precipitation occurs just before the maximum in surface pressure associated with the diurnal tide, but the maxima in the semidiurnal precipitation is associated with maxima in the rate of decrease of surface pressure.

Because theory suggests a strong forcing of the atmospheric tides (particularly the semidiurnal harmonic) by the diurnal cycle of heating in the stratosphere, it is possible to change the magnitude of the tides in this model by removing the diurnal variations in solar heating in the model stratosphere without directly changing the tropospheric heating rates (Fig. 3 shows the diurnal and semidiurnal harmonics of solar heating at the equator from the control integration). Any change in the diurnal cycle of precipitation in such an integration will highlight the role of the atmospheric tides in forcing the diurnal cycle of precipitation. Figure 4 shows the diurnal and semidiurnal harmonics of surface pressure and precipitation from an integration of the model in which the shortwave heating rates in the top five model levels

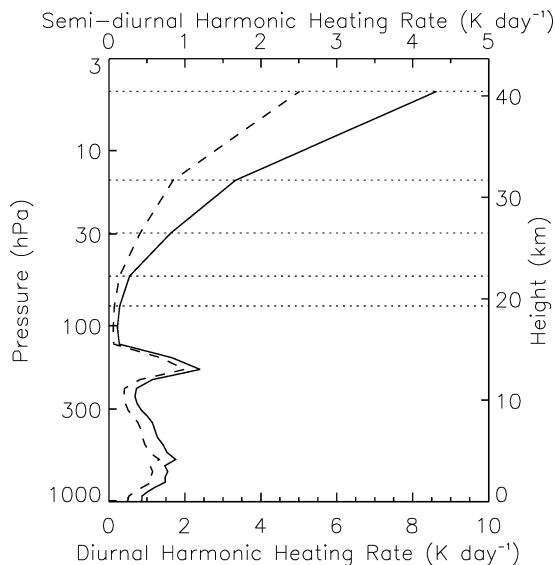


FIG. 3. The amplitude of the diurnal (solid line) and semi-diurnal (dashed line) harmonics of shortwave heating at the equator from the control integration of the model. The horizontal dotted lines show the levels at which the diurnal variations in heating are removed in the perturbation experiment. (The height coordinate is based on a scale height of 7.5 km.)

(shown by the horizontal dotted lines in Fig. 3) are overwritten by the time mean shortwave heating rates from the control integration of the model. Because the full radiation calculations are carried out at these levels (the calculated heating rates are just discarded), the shortwave radiation in the troposphere is unaffected by these changes. There is a small reduction, of about 15% in the amplitude of the diurnal tide when the diurnal variations in the stratospheric heating are removed. This small reduction is consistent with the strong tropospheric forcing of the diurnal tide predicted by theory. The semi-diurnal tide shows a larger reduction in amplitude of about 30%. However, this reduction is small in comparison to that which would be expected given the theoretical estimates reported in Chapman and Lindzen (1970) that approximately 70% of the semi-diurnal tide is forced by ozone heating. The results found here are in good agreement with those of a similar experiment by Hunt and Manabe (1968).

The discrepancies between the theoretical predictions and this numerical model, despite the apparent consistency of both with the observations, raises some questions about the forcing of the semi-diurnal tide. Either the theoretical predictions discussed in Chapman and Lindzen (1970) have overestimated the role of the stratosphere in generating the semi-diurnal tide and underestimated the role of the troposphere or the model's representation of the heating, or its response to it, is inaccurate. Because the semi-diurnal variations in solar heating are dominated by the progression of the sun, an incorrect representation of the semi-diurnal harmonic of solar heating in the model would also imply an inaccurate

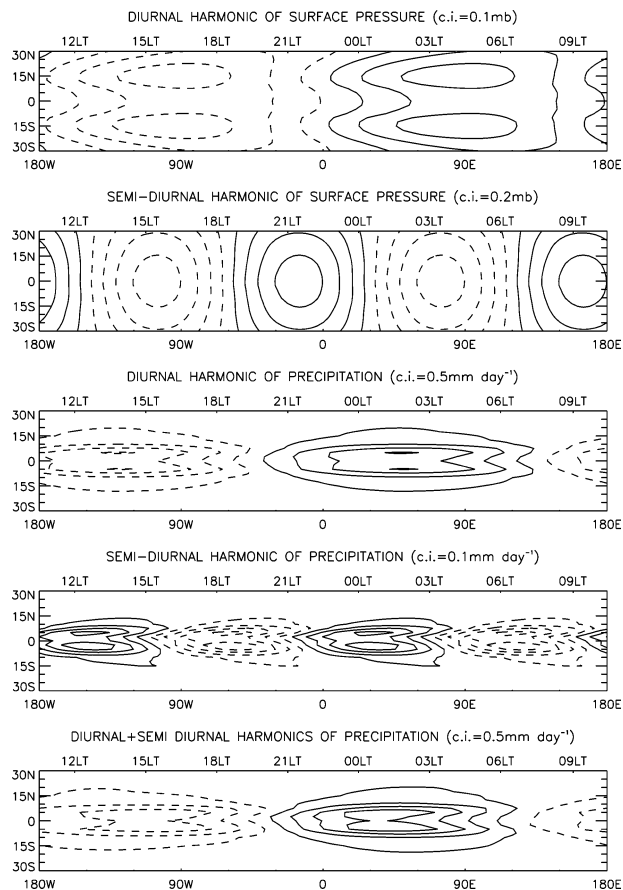


FIG. 4. As in Fig. 2 but for the integration with no diurnal variations of shortwave heating above 80 hPa. Note that the contour interval for the semi-diurnal harmonic of precipitation is half that in Fig. 2.

representation of the mean heating profile. This model has its top level at about 40 km, well below the maximum in ozone heating, and Zwiers and Hamilton (1986) showed that excluding the ozone heating above 10 hPa could lead to a 43% reduction in the amplitude of the semi-diurnal tide. However, the radiation scheme has been designed to account for the solar heating above these levels to ensure that the total column heating is correctly represented. It is possible that the poor representation of the vertical profile of the stratospheric heating in the model could be responsible for the weak forcing of the tides by the stratosphere in the model, but it cannot account for the relatively strong forcing from the troposphere that would be needed to compensate for this in giving the observed amplitude.

To probe the importance of tropospheric processes, an additional integration was performed in which the cloud radiative effects were removed in both longwave and shortwave heating by replacing the cloudy radiative heating profile with that computed for clear skies. Figure 5 shows the harmonics of surface pressure and precipitation for this integration. The surface pressure signal of the semi-diurnal tide in this case has an amplitude of

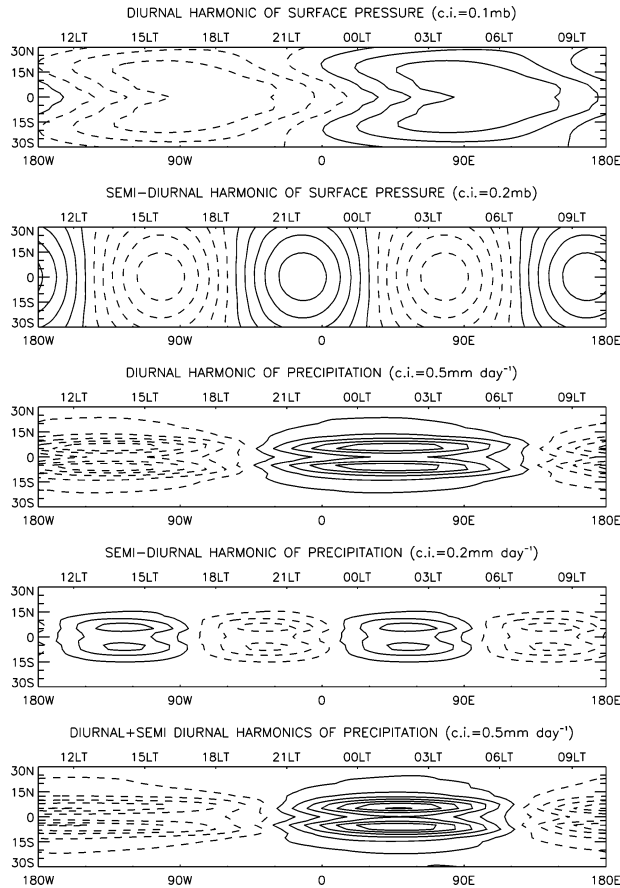


FIG. 5. As in Fig. 2 but for the integration with no cloud radiative effects. Contour intervals are as in Fig. 2.

1.05 hPa. This represents a reduction of only 10% compared with the control integration, indicating that the cloud radiative effects are not strong enough to compensate for the smaller impact of the ozone heating than in the predictions discussed in Chapman and Lindzen (1970).

In the aquaplanet GCM there must therefore be an enhanced response to the same thermal forcing, a stronger heating due to water vapor absorption or an additional heat source not included in the theory (e.g., long-wave radiation or latent heating). The vertical profile of shortwave heating in this model is indeed very different from that used in the results reported by Chapman and Lindzen (1970). In the aquaplanet model the maximum heating rates are at about 750 mb (Fig. 3) and are relatively uniform throughout the depth of the troposphere, in good agreement with radiative transfer models of the tropical atmosphere (e.g., Liou 1980). In contrast the profile shown in Chapman and Lindzen (1970, their Fig. 3.2) has its peak at the surface and decays exponentially with height. Such differences in vertical profile may account for some of the differences between theory and the model. Alternatively, Zwiers and Hamilton (1986) found that the presence of a rigid lid in the model am-

plified the surface pressure signal of the semidiurnal tide by about 30% due to the reflection of vertically propagating waves. It cannot be ruled out that some or all of the additional forcing or response required in this model to compensate for the apparently weak ozone forcing comes from such a spurious numerical mechanism.

In addition to the changes in the amplitude of the tides in the integration with no diurnal cycle of ozone heating there are changes in the diurnal cycle of precipitation. The diurnal harmonic of precipitation (Fig. 4) shows no change in phase as a result of the change in the amplitude of the tide, but does show some changes in amplitude. On the equator there is an increase in the magnitude of the diurnal harmonic of about 15% but, just off the equator (at about  $\pm 5^\circ$  where the mean precipitation is a maximum) there is a decrease in amplitude of about 5%. These changes are comparable in magnitude to the small changes that arise in the mean precipitation of the model between these two integrations as a result of the relatively short averaging periods for the statistics. It is difficult therefore to separate the role of the small changes in the diurnal tide from the impact of the small changes in the mean precipitation.

The semidiurnal harmonic of precipitation in this integration (Fig. 4) shows a much larger reduction in amplitude of between 40%–60% within the main tropical convective region, but with little or no change in phase. The maximum reduction occurs on the equator with the smallest changes occurring just off the equator where the mean precipitation has its maximum. The semidiurnal tide clearly plays a large role in determining the semidiurnal harmonic of precipitation in this model. The effect of these changes in the semidiurnal harmonic of precipitation is to give a diurnal cycle of precipitation that is more symmetric between its positive and negative phases.

The experiment with no cloud radiative effects (Fig. 5) shows only a small reduction in the magnitudes of the surface pressure harmonics compared with the control integration (about 10% for both diurnal and semidiurnal harmonics). However, there are significant changes to both diurnal and semidiurnal harmonics of precipitation in this integration. The diurnal harmonic of precipitation has a large increase in its maximum amplitude to  $2.7 \text{ mm day}^{-1}$ , but with very little change at the equator. However, the phase of the diurnal harmonic is relatively unaffected by the exclusion of the cloud radiative effects. The semidiurnal harmonic of precipitation shows a large reduction in magnitude on the equator to about  $0.4 \text{ mm day}^{-1}$ , but very little change off the equator; the phase of the semidiurnal harmonic in this integration is shifted to later in the day with maxima occurring at around 0200 and 1400 LT (cf. 0000 and 1200 LT for the control integration). However, the changes in the diurnal cycle of precipitation should be viewed in the context of the significant changes in the mean precipitation in this experiment. The equatorial

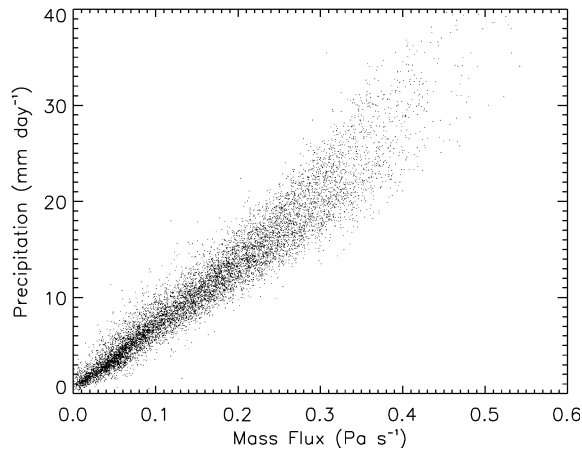


FIG. 6. Scatterplot of 3-hourly mean updraft mass flux at model level 10 (580 hPa) against precipitation for a sample of equatorial points for the control integration.

precipitation is reduced by 20% to  $8 \text{ mm day}^{-1}$  and the off-equatorial maxima are shifted poleward relative to the control integration with a much broader band of tropical convection. These changes to the mean climate of the model make it difficult to determine whether the changes in the diurnal cycle arise as a direct result of the absence of the cloud radiative effects or as an indirect effect associated with the change in the mean climate in this experiment.

#### 4. The convective response in the model

The results presented in section 3 indicate which aspects of the diurnal forcing might be responsible for driving the diurnal cycle of convection, but do not indicate how the convection scheme responds to the forcing. In this section a detailed analysis of the convective response to the diurnal forcing in the control integration will be presented. Section 4a describes some general aspects of the behavior of the convection scheme in this model. In sections 4b and 4c, the semidiurnal and di-

urnal harmonics of precipitation are investigated in the context of this behavior. Finally, section 4d describes the diurnal cycle of precipitation in experiments in which the convective closure was changed.

##### a. Behavior of the convection scheme

The convective precipitation in the aquaplanet version of HadAM3 shows variability on a range of time scales, from intraseasonal time scales down to the time step-by-time step variability typical of most convection schemes in GCMs. In order to discuss the processes that govern the diurnal variability of precipitation it is useful to determine some of the processes that govern the variability of precipitation on all of these time scales.

Figure 6 shows a scatterplot of the 3-hourly mean updraft mass flux at model level 10 (mean pressure 580 hPa) against the 3-hourly mean precipitation rates for a sample of one-sixth of the equatorial grid points. A clear relationship exists between the mass flux at this level and the precipitation. In fact the correlation coefficient between precipitation and mass flux at a given model level is in excess of 0.9 for levels 7 (733 hPa) to 18 (279 hPa) inclusive, with a maximum value of 0.97 at level 10. Similar relationships between the mass flux and the precipitation hold for the other latitudes within the model's tropical precipitation band. Given this strong relationship between mass flux and precipitation it would seem that the key to understanding variability in the precipitation, within the context of this convection scheme, is to understand the variability in midlevel updraft mass flux.

Figure 7a shows the time and zonal mean updraft mass flux profile from the convection scheme for the equatorial grid points. Also shown in Fig. 7b is the fraction of time steps at which there is a nonzero updraft mass flux at each level, based on a 10-day sample from nine equatorial grid points (a total of 4320 samples). At most time steps convection is initiated at level 1 and extends to model level 3, but only extends beyond level 3 about half of the time. Once the convection has pen-

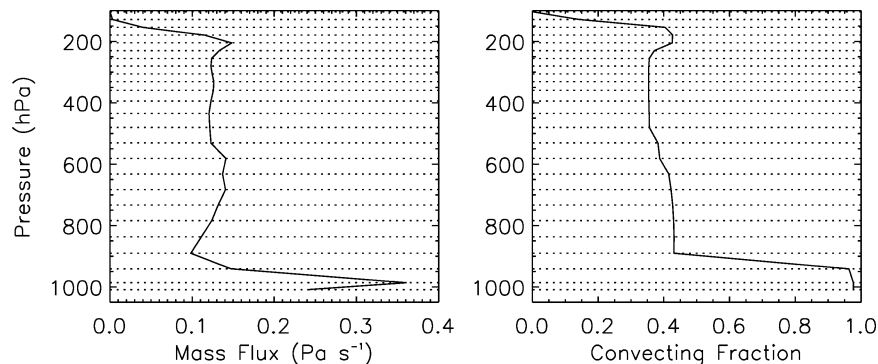


FIG. 7. (a) Zonal and time mean updraft mass flux from the convection scheme on the equator. (b) The fraction of grid points at which there is a nonzero updraft mass flux at that level. In both plots the dotted lines represent the location of the model levels.

etrated beyond level 3 (about 950 hPa), it generally extends throughout the depth of the troposphere with a small fraction (about 15% of the convection penetrating above level 3) terminating around the freezing level (550 hPa). The vertical profile of the mass flux and convecting fraction describes a modeled climate in which there is almost ubiquitous convection in the Tropics, with deep convection occurring about 50% of the time, but with very little variability in the depth of the deep convection. This is consistent with the warm pool regions of the western Pacific and Indian Oceans that the SST profile was designed to mimic.

For the buoyancy-based closure the midlevel mass flux is dependent on two quantities: First, it depends on the buoyancy excess as the parcel is lifted from the lowest convecting level (almost always model level 1 in this integration) to the next level, which controls the initial mass flux of the updraft. Second, the entrainment and detrainment profiles control the rate of change of the mass flux profiles with height.

The most important levels for determining the midlevel 3-hourly mean mass flux are the level at which the convection is initiated (and the initial mass flux is determined) and model level 3, which is where the shallow convection is capped in this integration. Whether the convection is shallow or deep and if it does extend beyond this layer, the strength of forced detrainment (and hence the mass flux above this level) will depend on the buoyancy of the lifted parcel at level 3.

The buoyancy of the convective parcel at any level will depend on the initial properties of the parcel, the properties of the air entrained from the levels during the ascent, and the properties of the environment at that level. It is therefore a function of many variables. This complexity can be reduced by considering the buoyancy of an undilute parcel, as this depends only on the initial parcel properties (which for this convection scheme are related to the environmental properties at the level at which the convection is initiated) and on the environmental properties at the level under consideration. The buoyancy of a such a pseudoadiabatically lifted parcel can be evaluated numerically; for the mean climatological profiles of humidity and temperature, a parcel lifted from the surface has a minimum buoyancy at model level 3. The minimum in the parcel buoyancy at this level means that this is a level that will be sensitive to perturbations in the buoyancy and hence is likely to be a significant level in determining whether the convection is shallow or deep, as well as the strength of any deep convection that occurs.

The analysis in the appendix gives an approximate expression for the perturbation buoyancy of a pseudoadiabatically lifted parcel as a function of perturbations in the environmental profiles of temperature and humidity. Warming or moistening the initial parcel, without changing the profile above, will lead to an increased buoyancy of the lifted parcel at levels above. However, for a vertically uniform profile of warming,

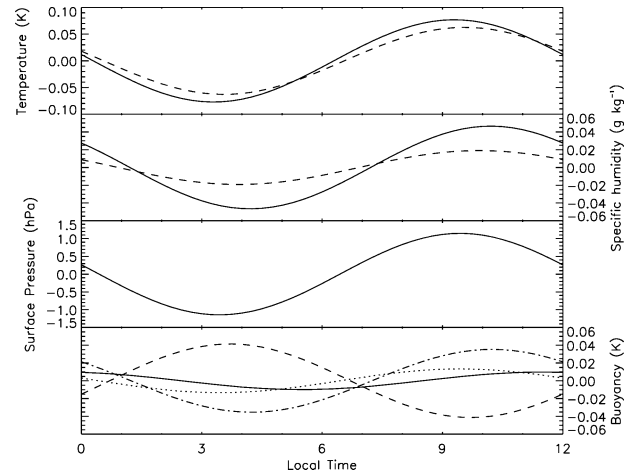


FIG. 8. The semidiurnal harmonics of (top) temperature, (second) humidity at model levels 1 (solid line) and 3 (dashed line), and (third) surface pressure from the control integration. (bottom) The effect of these variations on the buoyancy of a parcel lifted pseudoadiabatically from level 1 to level 3 (solid line) and the contributions from the temperature perturbations (dashed line), humidity perturbations (dotted line), and pressure perturbations (dash-dotted line). Note that only the period 0000–1200 LT is shown.

the buoyancy of a lifted parcel is reduced; the increase in temperature of the initial parcel is partly offset by the increase in lifting condensation level (and hence a reduction in the latent heating in the parcel).

This relationship between the parcel buoyancy and the environmental profile means that heating processes that lead to a near uniform warming of the lower troposphere will tend to decrease the buoyancy of the convective parcel at the top of the boundary layer and reduce the amount of convection that penetrates above this level.

#### b. The semidiurnal harmonic of precipitation

Given the behavior of the convection scheme described above, the semidiurnal variations in midlevel mass flux and, hence, the semidiurnal harmonic of precipitation will be strongly dependent on variations in the mass flux penetrating through the boundary layer (i.e., through level 3).

Figure 8 shows the semidiurnal harmonics of temperature and specific humidity at model levels 1 and 3 (corresponding to the levels at which the convection is initiated and the level at which the shallow convection typically terminates) and the surface pressure (because the model uses a  $\sigma$  coordinate in the vertical near the surface, the pressure variations at these levels are in phase with the surface pressure). Also shown is the effect of these variations on the parcel buoyancy at level 3 (as calculated by performing undilute parcel ascents with the perturbed profiles).

The semidiurnal variations in temperature at these levels (Fig. 8, top) are very similar in both magnitude

and phase. This relationship between the temperature at these two levels means that the dominant impact on the buoyancy of the temperature variations (dashed line in the bottom panel) is through variations in the height of the lifting condensation level (through changes in the relative humidity of the parcel). As the lowest level warms, the relative humidity decreases and the lifting condensation level increases, leading to a reduction in the buoyancy of a parcel lifted from the surface to model level 3 when the surface temperature is at a maximum. The specific humidity variations (second panel) lead to an increase in the buoyancy (dotted-dashed line in the bottom panel) for positive specific humidity variations through a lowering of the lifting condensation level. The buoyancy effects of the temperature and humidity are of similar magnitude (0.04 K) and are approximately out of phase. The semidiurnal variations in pressure (third panel) have a smaller effect on the buoyancy (dotted line in the bottom panel) than either the temperature or humidity effects, but have a comparable magnitude to the total buoyancy perturbation. The resulting buoyancy perturbation accounting for all of these effects has a magnitude of approximately 0.01 K with maximum just before noon and midnight local time. The maxima in buoyancy perturbations occur at the same time as the maxima in precipitation. The magnitude of the perturbations corresponds to 8% of the buoyancy of a parcel lifted through the time-mean environmental profile, compared with a magnitude of the semidiurnal harmonic of precipitation of 8.6% of the mean precipitation at the equator and a semidiurnal variation in the mass flux at level 4 of 8.6% of the mean mass flux at level 4.

Having diagnosed the variations in the profile that are responsible for the semidiurnal variations in precipitation we need to determine the processes that lead to the change in the temperature, humidity and pressure. Scale analysis of the linearized equations for the buoyancy perturbation shows that the sensitivity to the humidity variations at model level 3 is about one-third of that to the humidity variations at model level 1. As the humidity perturbations at level 3 shown in Fig. 8 are only one-third of the magnitude of those at level 1 they will not be considered further.

Figure 9 shows the semidiurnal variations of the temperature tendencies at model levels 1 and 3 and the humidity tendencies at level 1. For clarity, terms that have a magnitude less than 10% of the total have been excluded from the plots. The largest semidiurnal temperature tendency perturbation comes from the dynamical processes (which includes the advective tendencies and the adiabatic tendencies associated with pressure changes), but there are significant contributions from both the shortwave radiation and the convection at both levels, and longwave and boundary layer schemes at model level 1. The total humidity tendency is essentially the residual of large and nearly out of phase contributions from the convection and boundary layer schemes.

The large dynamical tendency of temperature arises as

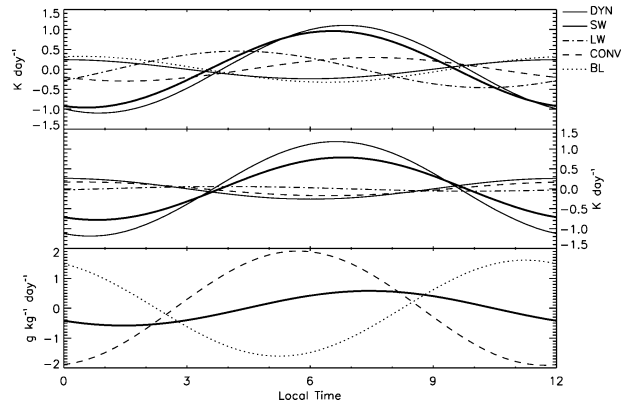


FIG. 9. The semidiurnal harmonics of the tendencies of (top) temperature at model level 1 and (middle) model level 3, and (bottom) specific humidity at model level 1 from the control integration (for a 12-h period only). The individual terms shown include the dynamics (DYN), shortwave radiation (SW), longwave radiation (LW), convection (CONV), and boundary layer scheme (BL); terms that are less than 10% of the total are not shown. The thick solid line shows the total tendency (including those terms that are not shown individually).

a result of the atmospheric semidiurnal tide shown in Fig. 2. The pressure signal associated with the semidiurnal tide arises predominantly through horizontal contraction and expansion of the atmospheric column. The pressure change  $\Delta p$  leads to a temperature change,  $\kappa T \Delta p / p$ . Substituting the observed magnitude of the aquaplanet's semidiurnal tide gives an amplitude of the semidiurnal harmonic of temperature due to the semidiurnal tide of about  $1.2 \text{ K day}^{-1}$ , which is comparable to the magnitude of the dynamics term shown in Fig. 9.

For the boundary layer variations that drive the semidiurnal harmonic of precipitation, the temperature can be thought of as being forced by factors that act independently of the convection, that is, the semidiurnal tide and the local radiative heating. In contrast the humidity variations are dominated by terms that arise as a result of the convection. The boundary layer scheme redistributes the strong drying of the lowest model level due to the convection throughout the depth of the boundary layer.

We now give a summary of the processes that generate the semidiurnal harmonic of convection in the model. The semidiurnal tide and semidiurnal variations in the radiation generate a temperature anomaly in the boundary layer that acts to increase the buoyancy of a parcel lifted to the top of the boundary layer, thereby increasing the amount of deep convection. However, the increase in deep convection tends to dry the boundary layer, which acts to decrease the buoyancy of the parcel and reduce the amount of deep convection. The competition between the temperature and humidity effects on the buoyancy means that the resulting buoyancy perturbation (and hence convective anomaly) is smaller than that which would occur due to temperature variations alone and causes the maximum in convection to

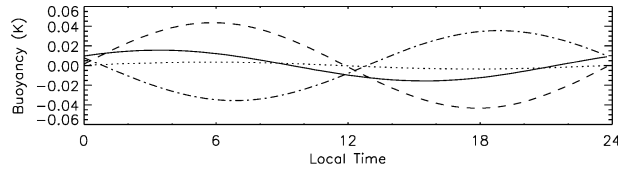


FIG. 10. The diurnal variations in buoyancy of a parcel lifted pseudoadiabatically from the surface to model level 3 (solid line) and the contributions to this buoyancy anomaly from the temperature (dashed line), humidity (dotted-dashed line), and pressure (dotted line) variations.

occur earlier than it would have in the absence of the humidity feedback.

### c. The diurnal harmonic of precipitation

A similar analysis can be performed for the diurnal harmonic of precipitation. The diurnal harmonic of the mass flux at model level 4 (the first level above the boundary layer) has a maximum at 0130 LT, the same time as the precipitation maximum. But, unlike the semidiurnal harmonic, the diurnal harmonic of convective mass flux shows small phase variations with height. The time of the maximum mass flux varies between 0100 and 0145 LT through the depth of the troposphere. These phase variations indicate that, in addition to processes in the boundary layer modify the mass flux out of the boundary layer, there are also variations in the free troposphere that affect the parcel ascent throughout the depth. However, the dominant mechanism controlling the diurnal harmonic of precipitation is again the variation in mass flux out of the boundary layer (i.e., through level 3). The variations in the mass flux profile arise because the longer time scale, compared to the semidiurnal harmonic, allows the diurnal variations of convection to modify the profile more and hence feedback on the convection.

Figure 10 shows the diurnal harmonic of the buoyancy at model level 3 for a parcel lifted pseudoadiabatically from the surface, arising from the diurnal harmonics of temperature, pressure, and humidity. The buoyancy of the pseudoadiabatically lifted parcel has a maximum at about 0300 LT, some  $1\frac{1}{2}$  h after the maximum in mass flux at level 4. This discrepancy suggests that either the mass flux variations at the top of the boundary layer are related to changes in the initial parcel mass flux (rather than the buoyancy variations at the top of the boundary layer) or that the assumption that the buoyancy variations can be explained by the pseudoadiabatic parcel ascent does not hold for the diurnal harmonic. Examination of the mass flux profile in the boundary layer reveals much smaller variability in the mass flux at level 3 than at level 4, suggesting that the variations in mass flux above the boundary layer are driven primarily by the amount of detrainment at level 3 rather than by changes in the mass flux at or below level 3. Variations in the modification of the parcel prop-

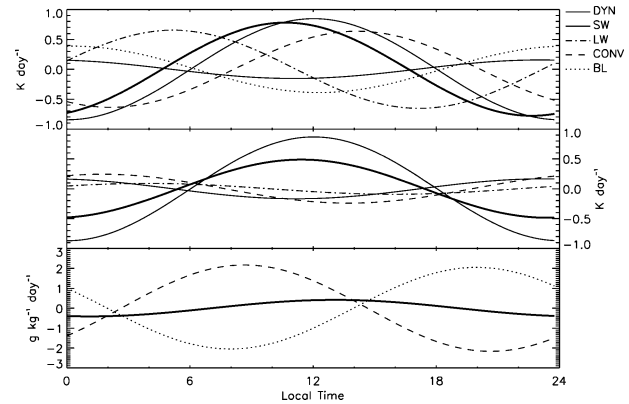


FIG. 11. The diurnal harmonic of the tendencies of temperature at (top) model level 1 and (middle) model level 3, and (bottom) specific humidity at model level 1 from the control integration. The individual terms shown include the dynamics (DYN), shortwave radiation (SW), longwave radiation (LW), convection (CONV), and boundary layer scheme (BL); terms less than 10% of the total are not shown. The thick solid line shows the total tendency (including those terms not shown individually).

erties by the entrainment are sufficient to slightly alter the phase of the buoyancy perturbation at the top of the boundary layer.

Figure 11 shows the diurnal harmonic of the tendencies of the low-level temperature and humidity. The source of the temperature variations within the boundary layer for the diurnal harmonic is less clearly dominated by an individual process than for the semidiurnal harmonic. The single largest term is the shortwave heating, which is in phase with the top-of-atmosphere radiation. The phase of the shortwave heating and the insensitivity of the phase of the diurnal harmonic of precipitation to the exclusion of the cloud radiative effects suggest that it is variations in the incoming solar radiation rather than changes in the vertical profile of absorption or reflection (i.e., by clouds or water vapor), which are important in determining the phase of the diurnal harmonic of precipitation, although the magnitude may be sensitive to changes in, for example, cloud cover. At model level 1 the diurnal harmonic in longwave radiation, convective, and boundary layer tendencies have similar magnitudes to those of the solar heating. In contrast to the semidiurnal tide, the dynamical forcing of the diurnal harmonic of temperature is small. As with the semidiurnal harmonic, the humidity variations at model level 1 are driven by large and nearly out of phase convective and boundary layer terms.

In summary, the processes that drive the diurnal harmonic of convection in the model are not as straightforward as for the semidiurnal harmonic. The net forcing of the boundary layer buoyancy is through a complicated balance of terms that act independently of the convection, such as the shortwave and longwave radiation (although even the phase of the longwave radiation variations may in part be determined by the phase of the convection through its effect on the temperature and

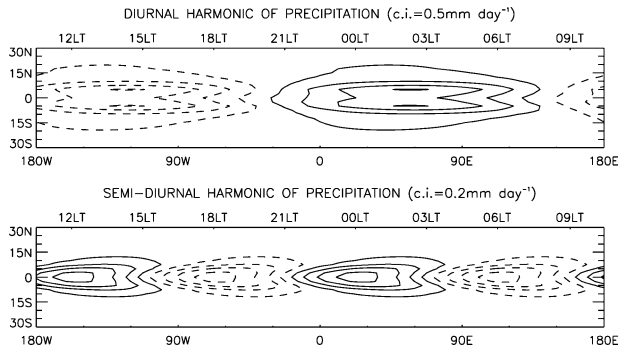


FIG. 12. Diurnal and semidiurnal harmonics of precipitation from the integration C1. The contour intervals are shown on the figure; for each plot the contours are offset from zero by half the contour interval, and the zero contour is not shown. Negative contours are dashed.

clouds) and those determined by the convection or processes strongly linked to it.

#### d. Sensitivity experiments

We have shown that a priori prediction of the phase and magnitude of the diurnal cycle in convection is difficult, even given a good understanding of the details of the individual components of the model. However, examining the sensitivity of the modeled diurnal cycle to changes in different components of the model parameterization schemes can suggest areas of study that could lead to improvements in the representation of the diurnal cycle of precipitation, and the representation of convection in general.

Figures 12–14 show the diurnal and semidiurnal harmonics of precipitation in integrations of the model with the alternative CAPE closure version of the convection scheme, rather than the buoyancy closure used in the control integration. The parcel ascent is performed in the same way for both versions of the convection scheme, but the initial mass flux is determined such that the convection acts to remove CAPE over a given time scale. Three experiments are shown in which the time scales for the destruction of CAPE are 1 h (experiment C1), 2 h (C2), and 4 h (C4). The experiment C1 (Fig. 12) behaves very much like the control integration, with the phase and magnitude of both the semidiurnal and diurnal harmonics of precipitation almost identical to those for the control integration. In an aquaplanet configuration the variety of forcing for convection is reduced compared to a GCM with a realistic surface specification, and it is possible for there to exist an approximately linear relationship between the buoyancy of a parcel at low levels and the CAPE in the profile. In such circumstances there can be a particular closure time scale for the convection that would produce a mass flux scaling equivalent to the buoyancy closure and, hence, the two integrations would be similar. For this particular setup this time scale appears to be close to 1 h. As well

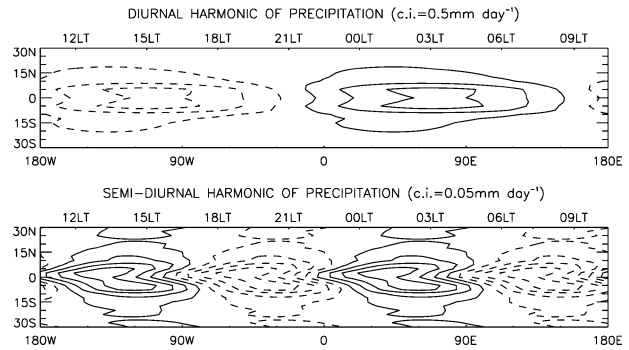


FIG. 13. As in Fig. 12 except for the C2 integration. Note that the contour interval for the semidiurnal harmonic is different from that in Fig. 12.

as the similar behavior for the diurnal cycle of convection, the climatology of the C1 and control integrations are very similar.

The C2 integration has a very different climatology from the control integration: The convective precipitation has a single peak on the equator (cf. the double peak of the control integration) and the maximum precipitation rate is increased. The strong relationship between the convective mass flux and the precipitation that exists in the control integration and the C1 integration is less marked in the C2 integration; the correlation between midtropospheric mass flux and the precipitation is of the order of 0.5 (cf. 0.95 for the control integration and C1). In this integration (Fig. 13) the diurnal harmonic of equatorial precipitation has a similar magnitude to that for the control integration, but this represents a smaller fraction of the daily mean precipitation compared to the control integration. Also, the phase is shifted to slightly later in the day. The semidiurnal harmonic shows a large absolute reduction in magnitude to about  $0.25 \text{ mm day}^{-1}$  (cf.  $0.75 \text{ mm day}^{-1}$  for the control integration) and also has a phase shift to later in the day.

Although the relationship between the precipitation and mass flux is much weaker for this integration, some

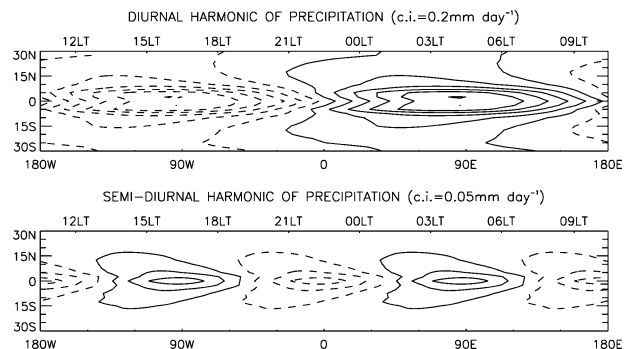


FIG. 14. As in Fig. 12 except for the C4 integration. Note that the contour intervals for both harmonics are different from that in Fig. 12.

of the variance in precipitation can be explained by variations in mass flux. The mean equatorial profile of this integration is such that there is no buoyancy minimum for a pseudoadiabatic parcel ascent at the top of the boundary layer, so the convection is less likely to terminate at the top of the boundary. In such circumstances the variations in mass flux are much more likely to be driven by variations in the initial mass flux. The variations in initial mass flux depend on the CAPE but, as this is an integrated measure of the buoyancy of a parcel lifted from the level at which the convection is initiated, it will still depend to some degree on the properties of the parcel and the environment in the same way as for the control integration. Because the time scale of the convection is longer than for the C1 integration, the precipitation response to a given forcing will be smaller, hence the reduction in the magnitude of the semidiurnal harmonic. This reduced sensitivity to the forcing will mean that the strength of the feedback due to the humidity variations, which are driven by the convection, will be reduced and the phase of the convection will shift closer to that forced by the temperature variations alone.

The C4 integration shows even greater differences in terms of its tropical climate. A significant component of tropical precipitation now comes from the large-scale precipitation scheme (about 20%) and there is increased large-scale cloud. The diurnal harmonic for the C4 integration (Fig. 14) shows a large reduction in magnitude (about 30%) compared to the C2 integration and a phase shift to later in the day. The semidiurnal harmonic, although it has a similar magnitude to the C2 integration, occurs later than would be expected from consideration of the response to the semidiurnal tide in the control, C1, and C2 integrations. These large changes in the diurnal cycle of convection reflect, in part, the large changes in the climatology of the model. In particular the presence of a significant amount of large-scale cloud in the Tropics will reduce the amplitude of the diurnal variability of the shortwave heating in the boundary layer as well as its mean.

## 5. Discussion and conclusions

The control integration of the aquaplanet version of HadAM3 has a realistic representation of the surface pressure signal of the diurnal and semidiurnal atmospheric tides, as well as a diurnal cycle of precipitation that is qualitatively in good agreement with the limited observations of the diurnal cycle of convection over the open tropical oceans. The results presented here provide an understanding of the basic response of the model's convection scheme to the diurnal forcing over the ocean and provide a basis for developing an understanding of the more complex system that includes the effects of, for example, land-ocean diurnal circulations or the diurnal cycle of sea surface temperature.

The diurnal cycle of the model precipitation has a

significant contribution from both the diurnal and semidiurnal harmonics. The diurnal harmonic in precipitation, with a peak in the early hours of the morning, is strongly forced by the diurnal harmonic of solar radiation. The semidiurnal harmonic is strongly forced by the semidiurnal atmospheric tide through the adiabatic temperature changes associated with the pressure variations, which lead to variations in the relative humidity in the boundary. The response to the semidiurnal pressure tide found here, with convection favored by the adiabatic expansion associated with divergence, is in contrast to the mechanism proposed by Dai et al. (1999) for the diurnal cycle of precipitation over the United States. They argued that the divergence associated with the diurnal pressure tide suppressed convection. The resultant phase of both of the diurnal and semidiurnal harmonics is strongly influenced by the convection through its impact on the humidity. The convective response to the diurnal forcing in the control integration arises primarily through the sensitivity of the proportion of deep and shallow convection to the boundary layer properties.

An experiment in which the cloud radiative effects were removed showed very little change in the phase of the diurnal harmonic of precipitation, although the phase of the semidiurnal harmonic did change. The relative insensitivity of the phase of the diurnal harmonic of precipitation in this integration suggests that, in this model at least, the cloud radiative effects do not play a significant role in determining the phase of the diurnal cycle of precipitation. The lack of impact of the cloud-radiative effects on the phase of the diurnal cycle of precipitation is in agreement with the results of a similar experiment reported by Randall et al. (1991). However, Randall et al. (1991) also reported a reduction in the amplitude of the diurnal cycle of convection in a "sea-world" integration in which the cloud radiative effects were removed, in contrast to the experiments reported here, which showed a large increase in the amplitude of the diurnal cycle when the cloud radiative effects were removed.

The sensitivity studies have shown that both phase and magnitude of the diurnal cycle of convection are sensitive to the closure of the convection scheme, but the changes in the climatology of the model make understanding the mechanisms through which this sensitivity arises difficult to determine. As observations of the oceanic diurnal cycle of precipitation improve, then comparisons between the observed and modeled diurnal cycle could provide some insight into the choice of convection parameterizations for GCMs.

An integration in which the diurnal cycle of stratospheric shortwave heating was removed highlighted some discrepancies between the theoretical description of the forcing of the semidiurnal tide and the modeled semidiurnal tide, which need further investigation. From the results presented in this paper, it can be hypothesized that

- 1) the water vapor shortwave absorption in the troposphere is deeper than in classical tidal theory and may therefore be more important in forcing the semidiurnal tide than previously thought,
- 2) stratospheric ozone heating may be rather less dominant in forcing the semidiurnal tide than previously thought, and
- 3) cloud radiative effects have a small impact on the forcing of the semidiurnal tide.

These results may be sensitive to the details of the representation of the stratosphere in the model and, in particular, the vertical profile of the ozone and the effects of the rigid lid boundary condition discussed by Zwiers and Hamilton (1986). As such they require further testing in a version of the model more suited to the task, that is, with a more realistic representation of the stratosphere including much better vertical resolution and an extended domain, and in more idealized experiments with imposed heating profiles. Nevertheless these experiments have demonstrated that the aquaplanet configuration provides an efficient framework for investigating the interaction between different components of the both the resolved and parameterized atmospheric processes. In particular, the study of a basic forced mode of variability, such as the diurnal cycle, has provided interesting information and highlighted some features of the sensitivity of the convection scheme, which may have more general implications for the variability of convection in the model.

*Acknowledgments.* The authors would like to thank Richard Lindzen and two anonymous reviewers for their helpful comments. S. J. Woolnough was supported by the Natural Research Council Grant NER/A/S/2000/1283. J. M. Slingo is funded by the NERC Centres for Atmospheric Science.

## APPENDIX

### The Buoyancy of a Pseudoadiabatically Lifted Parcel

Consider the variables that will affect the buoyancy of an undilute (for simplicity) parcel lifted from the lowest model level to a model level,  $k$ , above the lifting condensation level. The buoyancy perturbation,  $B_k$ , of a parcel lifted from level 1 to level  $k$  is defined by the model as

$$B_k = \theta_{vk}^p - \theta_{vk}^e = \left(\frac{p_0}{p_k}\right)^\kappa (T_{vk}^p - T_{vk}^e), \quad (\text{A1})$$

where  $T_v^p$  and  $T_v^e$  are the parcel and environmental virtual temperatures. Linearizing Eq. (A1) about a mean state such that, for example,  $B = \bar{B} + \Delta B$ , then the perturbation buoyancy  $\Delta B$  is given by

$$\Delta B_k = \left(\frac{\bar{p}_0}{\bar{p}_k}\right)^\kappa \left[ \Delta T_{vk}^p - \Delta T_{vk}^e - \kappa \frac{\Delta p_k}{\bar{p}_k} (\bar{T}_{vk}^p - \bar{T}_{vk}^e) \right]. \quad (\text{A2})$$

The virtual temperature is given by  $T_v = T(1 + \epsilon r)$ , where  $\epsilon = R_d/R_v$  and  $r$  is the humidity mixing ratio. To simplify the analysis the humidity mixing ratio in this equation is replaced by the specific humidity (although the calculations shown in section 3 will use the mixing ratio). This approximation is not expected to affect the qualitative results of the following analysis. Linearizing the approximated form of the virtual temperature gives

$$\Delta T_v = (1 + \epsilon \bar{q}) \Delta T + \bar{T} \Delta q. \quad (\text{A3})$$

The parcel temperature and humidity at model level  $k$  are given by

$$T_k^p = T_1^p \left(\frac{p_k}{p_1}\right)^\kappa + \frac{L_v}{C_p} (q_1^p - q_k^p), \quad (\text{A4})$$

$$q_k^p = q_s(T_k^p, p_k). \quad (\text{A5})$$

Linearizing Eqs. (A4) and (A5) gives

$$\begin{aligned} \bar{T}_k^p + \Delta T_k^p = & \left(\frac{\bar{p}_k}{\bar{p}_1}\right)^\kappa \left[ \bar{T}_1^p + \Delta T_1^p + \kappa \bar{T}_1 \left( \frac{\Delta p_k}{\bar{p}_k} - \frac{\Delta p_1}{\bar{p}_1} \right) \right] \\ & + \frac{L_v}{C_p} [\bar{q}_1^p + \Delta q_1^p - (\bar{q}_k^p + \Delta q_k^p)], \quad (\text{A6}) \end{aligned}$$

$$\Delta q_k^p = \Delta T_k^p \frac{\partial q_s}{\partial T} + \Delta p_k \frac{\partial q_s}{\partial p}. \quad (\text{A7})$$

This analysis will be applied at levels at which the vertical coordinate is  $(p/p_s)$ ; hence  $(\Delta p_k/p_k - \Delta p_1/p_1) \equiv 0$ . Using this expression in Eq. (A6) and rearranging gives

$$\begin{aligned} \Delta T_k^p = & \left( 1 + \frac{L_v}{C_p} \frac{\partial q_s}{\partial T} \right)^{-1} \\ & \times \left[ \left(\frac{\bar{p}_k}{\bar{p}_1}\right)^\kappa \Delta T_1^p + \frac{L_v}{C_p} \left( \Delta q_1^p - \Delta p_k \frac{\partial q_s}{\partial p} \right) \right]. \quad (\text{A8}) \end{aligned}$$

Substituting Eqs. (A7) and (A8) into the linearized equation for the virtual temperature [Eq. (A3)] and then into the equation for the perturbation buoyancy [Eq. (A2)] gives an expression for the perturbation buoyancy of a parcel lifted pseudoadiabatically from one level to another in terms of the environmental variables (assuming the initial parcel properties are related to the environmental profile).

The expressions can be simplified by considering the relative magnitude of the terms involving the pressure perturbations. At the levels of interest (i.e., where the parcel is only marginally buoyant)  $T_v^p - T_v^e \sim 0.2$  K and the term involving the pressure perturbation in Eq. (A2) will scale as  $0.2\kappa\Delta p_k/\bar{p}_k \sim 5 \times 10^{-7}\Delta p$  in the lower troposphere. The term involving the pressure per-

turbations in Eq. (A8), when substituted into the expression for the buoyancy perturbation, will scale as

$$\frac{L_v}{C_p} \frac{\partial q_s}{\partial p} \left( 1 + \frac{L_v}{C_p} \frac{\partial q_s}{\partial T} \right)^{-1} \Delta p \sim 10^{-4} \Delta p$$

for typical lower tropospheric values. Neglecting the pressure term in Eq. (A2) and dropping the overbar for mean values gives the following expression for the perturbation buoyancy:

$$\Delta B_k = \left( \frac{p_0}{p_k} \right)^\kappa \left[ \left( 1 + \epsilon q_k^p + T_k^p \frac{\partial q_s}{\partial T} \right) \Delta T_k^p + T_k^p \frac{\partial q_s}{\partial p} \Delta p_k - (1 + \epsilon q_k^E) \Delta T_k^E - T_k^E \Delta q_k^E \right], \quad (\text{A9})$$

where  $\Delta T_k^p$  is given by Eq. (A8).

In practice it is easier to calculate this buoyancy perturbation by performing a parcel ascent numerically rather than through this analysis. The advantage of having an analytical expression such as Eq. (A9) is that it enables an analysis of the source of the buoyancy perturbations.

#### REFERENCES

- Braswell, W. D., and R. S. Lindzen, 1998: Anomalous shortwave absorption and atmospheric tides. *Geophys. Res. Lett.*, **25**, 1293–1296.
- Chapman, S., and R. S. Lindzen, 1970: *Atmospheric Tides*. D. Reidel, 200 pp.
- Chen, S. S., and R. A. Houze, 1997: Diurnal variation and life-cycle of deep convective systems over the tropical Pacific warm pool. *Quart. J. Roy. Meteor. Soc.*, **123**, 357–388.
- Dai, A., 2001: Global precipitation and thunderstorm frequencies. Part II: Diurnal variations. *J. Climate*, **14**, 1112–1128.
- , and J. Wang, 1999: Diurnal and semidiurnal tides in global surface pressure fields. *J. Atmos. Sci.*, **56**, 3874–3891.
- , and K. E. Trenberth, 2004: The diurnal cycle and its depiction in the Community Climate System Model. *J. Climate*, **17**, 930–951.
- , F. Giorgi, and K. E. Trenberth, 1999: Observed and model-simulated diurnal cycles of precipitation over the contiguous United States. *J. Geophys. Res.*, **104**, 6377–6402.
- Gray, W. M., and R. W. Jacobson, 1977: Diurnal variation of deep cumulus convection. *Mon. Wea. Rev.*, **105**, 1171–1188.
- Gregory, D., and P. R. Rowntree, 1990: A mass flux convection scheme with the representation of cloud ensemble characteristics and stability-dependent closure. *Mon. Wea. Rev.*, **118**, 1483–1506.
- , and S. Allen, 1991: The effect of convective scale downdrafts upon NWP and climate simulations. Preprints, *Ninth Conf. on Numerical Weather Prediction*, Denver, CO, Amer. Meteor. Soc., 122–123.
- , R. Kershaw, and P. M. Inness, 1997: Parameterization of momentum by convection. II: Tests in single column and general circulation models. *Quart. J. Roy. Meteor. Soc.*, **123**, 1153–1183.
- Hamilton, K., 1981: Latent heat release as a possible forcing mechanism for atmospheric tides. *Mon. Wea. Rev.*, **109**, 3–17.
- Haurwitz, B., 1956: The geographical distribution of the solar semidiurnal pressure oscillation. New York University Meteorology Paper, Vol. 2 (5), 36 pp.
- , 1965: The diurnal surface pressure oscillation. *Arch. Meteor. Geophys. Bioklimatol.*, **A14**, 361–379.
- Hunt, B. G., and S. Manabe, 1968: An investigation of thermal tidal oscillations in the earth's atmosphere using a general circulation model. *Mon. Wea. Rev.*, **96**, 753–766.
- Inness, P. M., J. M. Slingo, S. J. Woolnough, R. B. Neale, and V. D. Pope, 2001: Organization of tropical convection in a GCM with varying vertical resolution: Implications for the simulation of the Madden-Julian oscillation. *Climate Dyn.*, **17**, 777–793.
- Janowiak, J. E., P. A. Arkin, and M. Morrissey, 1994: An estimation of the diurnal cycle in oceanic tropical rainfall using satellite and in situ data. *Mon. Wea. Rev.*, **122**, 2296–2311.
- Li, D., and K. Shine, 1995: A 4-dimensional ozone climatology for UGAMP models. UGAMP Internal Note 35, United Kingdom Universities Global Atmospheric Modelling Programme, Department of Meteorology, University of Reading, Reading, United Kingdom, 43 pp.
- Lindzen, R. S., 1978: Effect of daily variations of cumulonimbus activity on the atmospheric semidiurnal tide. *Mon. Wea. Rev.*, **106**, 526–533.
- Liou, K.-N., 1980: *An Introduction to Atmospheric Radiation*. Academic Press, 392 pp.
- McGarry, M. M., and R. J. Reed, 1978: Diurnal variations in convective activity and precipitation during phases II and III of GATE. *Mon. Wea. Rev.*, **106**, 101–113.
- Nesbitt, S. W., and E. J. Zipser, 2003: The diurnal cycle of rainfall and convective intensity according to three years of TRMM measurements. *J. Climate*, **16**, 1456–1475.
- Pope, V. D., M. L. Gallani, P. R. Rowntree, and R. A. Stratton, 2000: The impact of new physical parametrizations in the Hadley Centre climate model—HadAM3. *Climate Dyn.*, **16**, 123–146.
- Randall, D. A., Harshvardhan, and D. A. Dazlich, 1991: Diurnal variability of the hydrologic cycle in a general circulation model. *J. Atmos. Sci.*, **48**, 40–62.
- Slingo, A., K. I. Hodges, and G. J. Robinson, 2004: Evaluation of the simulation of the diurnal cycle in a climate model using data from *Meteosat 7*. *Quart. J. Roy. Meteor. Soc.*, **130**, 1449–1467.
- Sui, C.-H., K.-M. Lau, Y. N. Takayabu, and D. A. Short, 1997: Diurnal variations in tropical oceanic convection during TOGA COARE. *J. Atmos. Sci.*, **54**, 639–655.
- Woolnough, S. J., J. M. Slingo, and B. J. Hoskins, 2001: The organisation of tropical convection by intraseasonal sea surface temperature anomalies. *Quart. J. Roy. Meteor. Soc.*, **127**, 887–908.
- Yang, G.-Y., and J. M. Slingo, 2001: The diurnal cycle in the Tropics. *Mon. Wea. Rev.*, **129**, 784–801.
- Zwiers, F., and K. Hamilton, 1986: Simulation of solar tides in a Canadian Climate Centre general circulation model. *J. Geophys. Res.*, **91**, 11 877–11 896.